RSC Advances

PAPER

View Article Online
View Journal | View Issue

Cite this: *RSC Adv.*, 2017, **7**, 50739

Characteristics of mechanical properties of sulphur cross-linked guayule and dandelion natural rubbers†

P. Junkong,[a] K. Cornish[b] and Y. Ikeda *[c]

Roles of non-rubber components in guayule and dandelion natural rubbers on the mechanical properties of each sulphur cross-linked rubber are revealed for the first time by analysing the Mullins effect, dynamic mechanical properties and strain-induced crystallization (SIC) from a new viewpoint, in comparison with sulphur cross-linked *Hevea* natural rubber (S-NR) and synthetic isoprene rubber (S-IR). Physically aggregated non-rubber components, particularly proteins, work as "natural reinforcing fillers". Higher-order structures of the physically aggregated non-rubber components in guayule (S-GR) and dandelion (S-DR) natural rubber matrices are proposed on the basis of their characteristic mechanical responses and SIC phenomena. Soft aggregates in S-GR accelerated the orientation of rubber chains and further development of SIC. The stronger physically aggregated non-rubber components, especially proteins in S-DR, accelerated SIC at the beginning of stretching, but impeded the orientation of rubber molecules with further stretching, resulting in the less development of SIC. This was also seen to a lesser degree in S-NR. The physical interaction of the aggregates of non-rubber components in dandelion natural rubber was suggested to be weaker than that in *Hevea* natural rubber. These phenomena could explain the characteristics of generated strain-induced crystallites during deformation in all samples, which clearly support the concept of "template crystallization" for SIC phenomena. SIC is a key parameter which should be considered in order to effectively utilize guayule and dandelion natural rubbers as alternatives for *Hevea* natural rubber in rubber industry.

Received 2nd August 2017
Accepted 23rd October 2017

DOI: 10.1039/c7ra08554k

rsc.li/rsc-advances

Introduction

Natural rubber (NR) from *Hevea brasiliensis* is a necessity for many industrial and household applications. Especially, it is required for heavy-duty tires, essential components of vibration isolation structures against earthquakes, and medical products.[1–3] This versatility of *Hevea* NR is ascribed to its toughness, outstanding tensile properties, and excellent crack growth resistance, which are assumed to be due to its ability to crystallize upon stretching, namely its strain-induced crystallization (SIC) behaviour.[4–14] However, the production capacity of *Hevea* NR is restricted to tropical regions, and research on alternatives has largely focused on the synthesis of its synthetic analog (*cis*-1,4-polyisoprene, IR). There are major differences between *Hevea* NR and IR. For example, the rubber component of *Hevea* NR is 100% *cis*-1,4 structure of polyisoprene apart from two *trans* units on the initial end,[15] but the highest achieved in IR is 98.5% in IR2200.[16] Additionally, solid *Hevea* NR contains a few percent non-rubber components, such as proteins, phospholipids, carbohydrates and metal ions,[15] whereas IR does not contain impurities. In spite of the very similar chemical structures of *Hevea* NR and IR, vulcanized IR exhibits weaker tensile strength and tearing resistance than vulcanized *Hevea* NR.[17] Therefore, studies on rubber yielding plants other than *Hevea* have been resumed to meet the NR requirements of this century.[4,5,18–20]

Guayule (*Parthenium argentatum*) and rubber dandelion (*Taraxacum kok-saghyz*, also known as rubber root, Russian dandelion, Kazak dandelion, Buckeye Gold, TKS and TK) have long been known to produce NR, and are the most promising species for the next-generation of NR sources.[21–27] Up to now, studies have focused on mechanical properties, such as tensile properties,[28–31] tear strength,[30] hardness,[30] fatigue life,[32,33] dynamic mechanical properties,[34] compression set[35] and rebound properties[30] of cross-linked and uncross-linked guayule NR compared to various kinds of rubber in both filled and unfilled systems. Recently, uncross-linked guayule NR, and guayule NR from which the rubber particle membranes were

[a]*Graduate School of Science and Technology, Kyoto Institute of Technology, Matsugasaki, Sakyo, Kyoto 606-8585, Japan*

[b]*Departments of Food, Agricultural and Biological Engineering, and Horticulture and Crop Science, Ohio Agricultural Research and Development Center, The Ohio State University, Wooster, OH 44691, USA*

[c]*Center for Rubber Science and Technology, Faculty of Molecular Chemistry and Engineering, Kyoto Institute of Technology, Matsugasaki, Sakyo, Kyoto 606-8585, Japan. E-mail: yuko@kit.ac.jp*

† Electronic supplementary information (ESI) available: An example of the template crystallization of cross-linked natural rubber. See DOI: 10.1039/c7ra08554k

stripped before rubber solidification, showed similar glass transition temperatures (T_g) to uncross-linked *Hevea* NR.[34] However, the storage moduli at 25 °C of the two guayule NRs were lower than that of *Hevea* NR. Both could be explained by their lower branching and gel content compared with *Hevea* NR, which leads to less chain entanglement.[34] Until now, the mechanical properties of dandelion NR are little reported.

The SIC of guayule NR has been investigated: for example, uncross-linked guayule NR showed a lower degree of crystallinity than uncross-linked *Hevea* NR, but was still higher than uncross-linked IR containing 93% or 97% of *cis*-content.[36] However, the crystallinity degree became higher in guayule NR than *Hevea* NR when both were cross-linked using peroxide.[37] These results were obtained from birefringence measurements of pre-stretched samples with a very long exposure time of light (3 h) to the samples. Therefore, the SIC behaviours may have contained significant stress relaxation effects because of the lengthy, non-real time measurement during stretching. The stress relaxation phenomenon also was observed in the SIC behaviour of uncross-linked dandelion NR investigated by wide-angle X-ray diffraction (WAXD) during slow deformation.[38] Recently, Ikeda *et al.* described the SIC behaviours of sulphur cross-linked (vulcanized) guayule, dandelion and *Hevea* NRs by using quick time-resolved simultaneous synchrotron WAXD measurement during tensile deformation *in situ*.[39] The SIC behaviours of cross-linked dandelion NR were comparable to cross-linked *Hevea* NR. Upon high stretching, the cross-linked guayule NR showed a superior SIC to cross-linked *Hevea* and dandelion NRs. When these three samples were compared, their SIC behavioural differences were speculated to be caused by the specific macromolecular structures and the amounts of non-rubber components. The unique SIC properties of cross-linked guayule NR compared to cross-linked *Hevea* and dandelion NRs were concluded to be due to its less branched physical network structure, which may be caused by lower non-rubber proteins and other components. The results of a comparative study between sulphur cross-linked guayule NR and IR also suggest that non-rubber components formed cross-linked sites which, in combination with the high regularity of *cis*-1,4-polyisoprene configuration of guayule, accelerate SIC.[40] The influence of non-rubber components on the SIC behaviours of uncross-linked *Hevea* NR[41–44] led to claims that the non-rubber components in *Hevea* NR may generate a pseudo end-linked network which allows uncross-linked NR to be crystallized under strain.[43,44] However, this seems insufficient to explain the SIC behaviours of guayule and dandelion NRs, even though studies on their non-rubber components have been performed.[34,45–51]

Specifically, SIC behaviours of the sulphur cross-linked rubbers should be evaluated because most of the rubber products used nowadays are produced using a sulphur cross-linking reaction (vulcanization). Note that guayule and dandelion NRs are purified in order to remove resins from the rubbers, because the presence of resins is known to accelerate oxidation, degrade the rubber, retard the vulcanization reaction of rubber and so on.[28,39,40] Because the resins are insoluble in water but soluble in polar organic solvents, acetone extraction has been widely used for this purpose.[24,28,29,39,40,46,48,50] In this paper, guayule and dandelion NRs are subjected to acetone purification before sulphur cross-linking. The roles of non-rubber components on dynamic mechanical properties and the cyclic tensile properties of sulphur cross-linked guayule and dandelion NRs are investigated and combined with the characteristics SIC from a new point of view, using our previous data of quick *in situ* simultaneous synchrotron time-resolved WAXD/tensile measurements.[39,40] Comparisons with the results of sulphur cross-linked *Hevea* NR and IR newly show unique characteristics of guayule and dandelion NRs, which may affect their utility as alternatives to *Hevea* NR.

Experimental section

Materials

Coagulated guayule and dandelion NRs were obtained from The Ohio State University, Ohio Agricultural Research and Development Center (OARDC). The rubbers were subjected to a conventional acetone extraction to remove resins.[24,28,29,39,40,46,48,50] Additionally, a commercial grade *Hevea* NR (RSS no. 1)[52] and synthetic isoprene rubber (IR2200, supplied from JSR Co.) were used as reference samples after acetone extraction. Amounts of acetone soluble components in guayule NR, dandelion NR, *Hevea* NR and IR were 14.4%, 15.6%, 2.6% and 1.3%, respectively. All purified rubbers were subjected to elemental analysis at the Center for Organic Elemental Microanalysis, Kyoto University: % C atom (guayule NR: 86.8, dandelion NR: 83.9, *Hevea* NR: 86.0 and IR: 86.8), % H atom (guayule NR: 11.8, dandelion NR: 11.7, *Hevea* NR: 11.6 and IR: 11.8), and % N atom (guayule NR: 0.0, dandelion NR: 0.8, *Hevea* NR: 0.6, IR: 0.0).

Assignment of FT-IR spectra for the purified rubbers (Fig. 1): 3038 cm^{-1} (olefinic C–H stretching), 2960–2850 cm^{-1} (alkyl C–H stretching), 1664 cm^{-1} (C=C stretching), 1450 cm^{-1} ($-CH_2$ symmetrical stretching, CH_3 asymmetrical stretching), 1375 cm^{-1} (C–H symmetrical bending) and 840 cm^{-1} (olefinic C–H out of plane bending). Non-rubber components were assigned to the following. (1) 3450 cm^{-1} (O–H symmetrical stretching), (2) 3280 cm^{-1} (N–H symmetrical stretching of secondary amide), (3) 1544 cm^{-1} (N–H bending of mono-substituted amide II), (4) 1622 cm^{-1} (C=O stretching of mono-substituted amide I), (5) 1694 cm^{-1} (C=O asymmetrical stretching of dimer of acid) and (6) 1738, 1736 and 1735 cm^{-1} (C=O asymmetrical stretching of ester for purified dandelion, *Hevea* and guayule NRs, respectively). Relative intensities of absorption bands for the C=O stretching of acids and esters against the band of $-CH_2$ rocking of polyisoprene at 740 cm^{-1} were in the order of dandelion NR > *Hevea* NR > guayule NR, and those for N–H stretching in peptide bond and amide I & II were larger in dandelion NR than in *Hevea* NR. In addition, sugars (mono- and polysaccharides) observed in purified *Hevea* and dandelion NRs were clearly assigned in their FT-IR spectra after subtraction by spectrum of isoprene rubber as shown in Fig. 1(c). For purified *Hevea* and dandelion NRs: (7) 1074 (broad shoulder peak), (8) 1105, (9) 1122 and (10) 1155 (broad peak) cm^{-1} (C–O–C asymmetrical stretching of alkyl substituted ether and/or cyclic

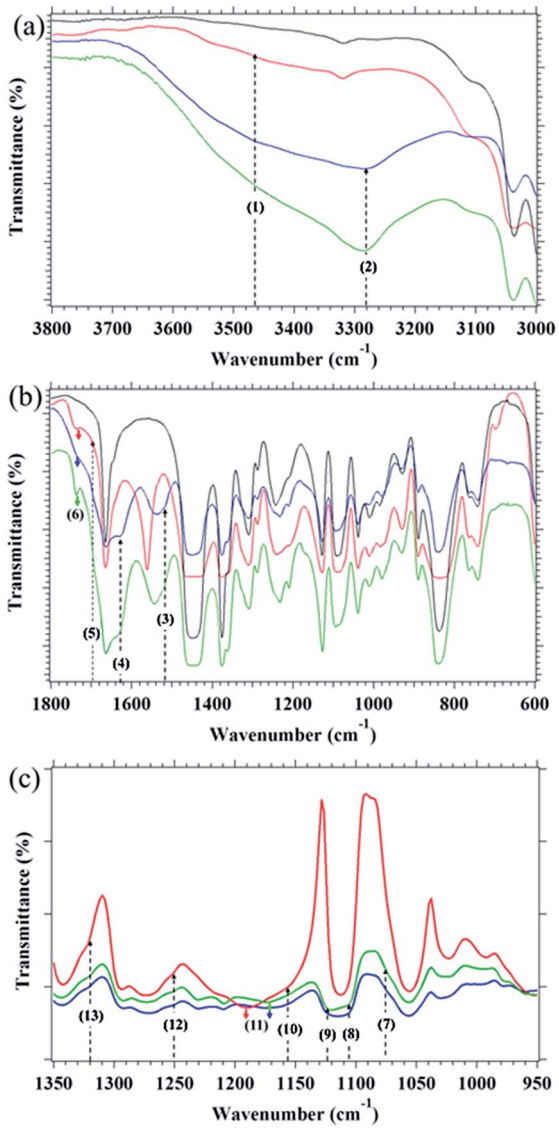

Fig. 1 FT-IR spectra of the purified guayule (—), rubber dandelion (—) and *Hevea* (—) natural rubbers, and isoprene rubber (—) after acetone purifications in the transmittance mode at r.t. in the range of (a) 3800–3000 cm^{-1} and (b) 1800–600 cm^{-1} and (c) FT-IR spectra of purified natural rubber samples in the range of 1350–1000 cm^{-1} after subtraction with isoprene rubber.

ethers), (11) 1174 cm^{-1} (C–O stretching in hydroxyl groups), (12) 1252 and (13) 1323 cm^{-1} (–O–H bending of hydroxyl groups). Peaks of (1)–(13) were not detected in purified isoprene rubber. The FT-IR measurements for all purified rubbers were carried out at 64 scans every about 88 s in a wavenumber range from 4000 to 400 cm^{-1} at room temperature (r.t.) using a transmittance method with a Shimadzu Infrared Prestige-21. The details of raw materials and description of the acetone extraction were explained in a previous paper.[39]

Each purified rubber was subjected to sulphur cross-linking (vulcanization) as follows.[39] Zinc oxide (ZnO) of 1.0 parts per one hundred rubber by weight (phr), 2.0 phr stearic acid, 1.0 phr *N*-cyclohexyl-2-benzothiazole sulfenamide (CBS) and 1.5 phr sulphur were mixed with rubber by using a conventional two-roll mill (6 × 15 test roll, Kansai Roll Co., Ltd., Osaka, Japan). Elemental sulphur (powder, 150 mesh), stearic acid (LUNAC S-25), ZnO (average diameter 0.29 μm) and CBS (Sanceler CM-G) were commercial grades for rubber processing and used as received. They were purchased from Hosoi Chemical Industry Co., Ltd., Kao Co., Sakai Chemical Industry Co., Ltd., and Sanshin Chemical Industry Co., Ltd., respectively. The rubber compounds obtained were cured at 140 °C in a mold to make 1 mm thick cross-linked rubber sheets. The press-heating times for guayule NR, dandelion NR, *Hevea* NR and IR were 15, 17, 14 and 26 min, respectively, which were determined from the maximum torques in the cure curves obtained at 140 °C using the JSR Curelastometer III as shown in Fig. 2. Hereafter, the sulphur cross-linked samples are designated as S-GR, S-DR, S-NR and S-IR for guayule, dandelion and *Hevea* natural rubbers, and synthetic isoprene rubber, respectively. Their raw (not vulcanized, but purified) rubbers are referred to as guayule natural rubber, dandelion natural rubber, *Hevea* natural rubber, and isoprene rubber, respectively. The network-chain densities of the cross-linked rubbers calculated by the modified Flory–Rehner equation,[53] using the results of swelling test in toluene at 25 °C, are shown in Table 2.

Simultaneous cyclic tensile and synchrotron time-resolved WAXD measurements

Cyclic tensile measurements were performed on ring-shaped samples using a tailor-made tensile tester (ISUT-2201, Aiesu Giken, Co., Kyoto, Japan) during the synchrotron WAXD measurement at approximately 25 °C in SPring-8. The samples were subjected to seven uniaxial loading–unloading cycles with a given stretching ratio (α) ranging from 2.0 to 8.0. Seven cycles of loading–unloading from zero stress (σ) up to the maximum strain and then down to zero stress again. Outside and inside diameters of the ring-shaped samples were 13.7 and 11.7 mm, respectively. Here, α is defined as $\alpha = l/l_0$, in which l_0 is the initial length and l is the length after deformation. The stretching speed was 100 mm min^{-1}, *i.e.*, the strain speed was

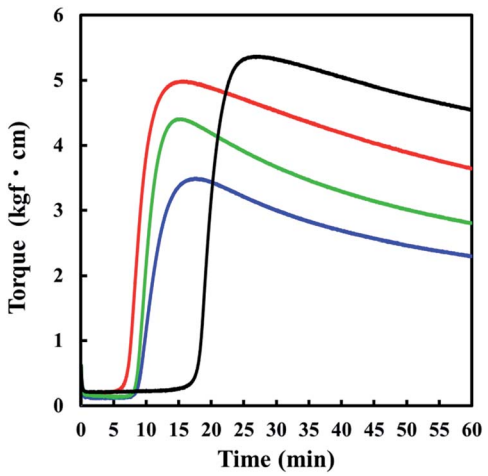

Fig. 2 Cure curves of S-GR (—), S-DR (—), S-NR (—) and S-IR (—) at 140 °C.

about 4.98 per min. The wavelength of the X-ray was 0.08322 nm and the camera length was 131 mm. Intensity of the incident X-ray was attenuated using an aluminum plate equipped on the beamline. The sample was exposed to the incident beam for 70 ms every 3 s. The two-dimensional WAXD patterns were recorded using a CCD camera (HAMAMATSU ORCA II). In this paper, only the cyclic tensile data are discussed, and some of WAXD patterns are only shown together with the cyclic tensile properties.

Dynamic mechanical analysis (DMA)

Dynamic mechanical properties were evaluated using a Rheospectolar DVE-4 instrument in a tension mode at a frequency of 10 Hz and temperature range from −130 °C to 150 °C at a heating rate of 2 °C per min. The size of the specimen was 25 × 5 × 1 in mm^3. The applied static force was automatically controlled, and the dynamic strain was ±3 μm. Storage modulus (E') and loss factor (tan δ) were measured as a function of temperature.

Differential scanning calorimetry (DSC)

DSC measurement was carried out using a Rigaku Thermoflex (DSC-8230) under a nitrogen atmosphere. The temperature was controlled from −130 °C to 150 °C at a heating rate of 10 °C per min after setting the sample at 35 °C for about 10 min. The amount of the sample mass was about 10 mg encapsulated in an aluminium pan.

WAXD analyses of SIC behaviours against stress under monotonic uniaxial deformation

Three structural parameters, "crystallinity index (CI)", "oriented amorphous index (OAI)" and "oriented index (OI)" of S-GR, S-DR, S-NR and S-IR from the previous publications[39,40] were reused to investigate the effect of non-rubber components on SIC behaviours. Apparent crystallite sizes (L_{hkl}), orientation fluctuations (β_{az}), average volume of crystallites (V_c) and index of average number of the crystallites per unit volume (N)[39,40] also were reused in this study. For the new point of view, the orientation and crystallization rate indexes were calculated as "(slope in the strain dependence of CI or OAI) × (strain speed)". Lattice constants (a, b, and c) of the samples were determined using the WAXD patterns by the least-squares regression method.[8,54] The volume per unit cell was calculated using a, b and c values.

The WAXD data were obtained by simultaneous monotonic tensile and synchrotron time-resolved WAXD measurements at the BL-40XU beamline of SPring-8 in Harima, Japan. The data were analysed using "POLAR" (Stonybrook Technology &Applied Research, Inc.).[8,54]

Results and discussion

Tensile characteristics under successive cyclic uniaxial deformation

Stress–strain curves of S-GR, S-DR, S-NR and S-IR under repeated cyclical conditions are shown in Fig. 3. All stress–strain curves

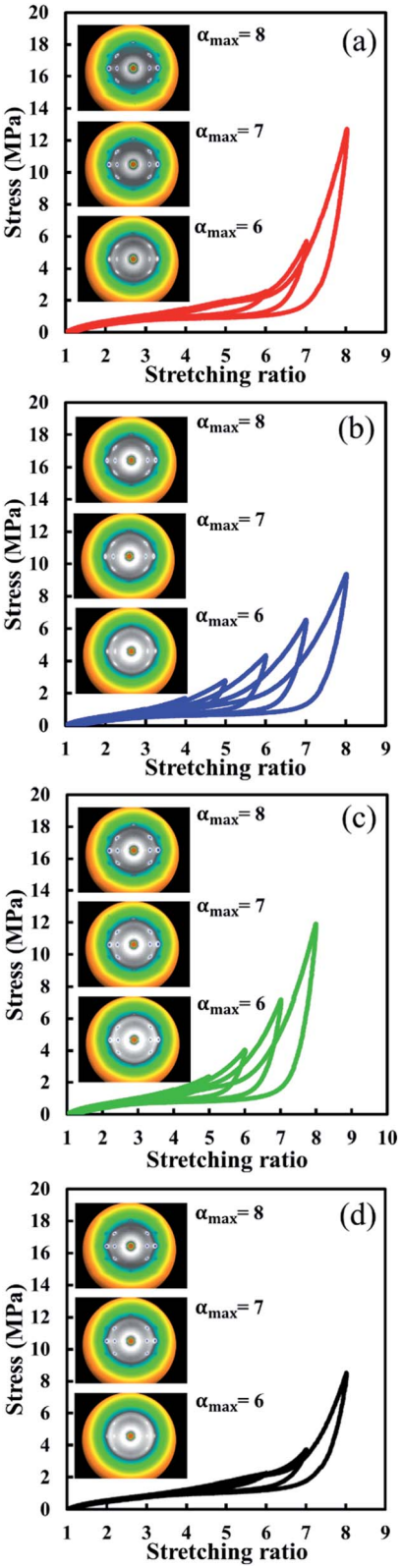

Fig. 3 Stress–strain curves of (a) S-GR, (b) S-DR, (c) S-NR and (d) S-IR under the successive cyclic deformation at the different maximum stretching ratios.

were obtained during simultaneous tensile/WAXD measurements. Here, two-dimensional WAXD patterns at $\alpha_{max} = 6.0$, 7.0 and 8.0 are shown together with their stress–strain curves for all the samples. The crystalline reflections in the WAXD patterns of S-GR, S-DR, S-NR and S-IR (Fig. 3) suggest reproducibility of their SIC behaviours when subjected to several repeated cycles. In general, the Mullins effect refers to a stress softening, characterized by a lower resulting stress for the same applied strain, which significantly appears after the first loading in rubber materials. Then, the subsequent loading closely follows the first unloading curve and shows a much less softening degree as long as the previous maximum strain is not exceeded.[55–57] In our study, a stress softening in S-IR was not observed in any cycle until it was extended to $\alpha_{max} = 8.0$, indicating the mostly fully elastic behaviour of S-IR. Although S-GR contained some physically aggregated non-rubber components, it surprisingly had a very low stress softening degree, similar to S-IR. However, the degree of stress softening at the last stretching process ($\alpha_{max} = 8.0$) of S-GR was greater than that of S-IR. This may be due to the more accelerated SIC behaviour of S-GR than S-IR ascribed to the higher regularity of *cis* configuration of guayule natural rubber than isoprene rubber.

On the other hand, the stress softening of S-DR and S-NR started at an earlier strain, $\alpha_{max} = 4.0$ and 6.0, respectively. Also, the degree of stress softening at the same stretching ratio, *e.g.* $\alpha = 7.0$, of S-DR and S-NR were 31% and 27%, which were higher than those of S-IR and S-GR, being 11% and 12%, respectively. Additionally, the degree of stress softening in both S-DR and S-NR was found to progressively increase with increasing α_{max}. Since S-IR did not show a clear Mullins effect, but did have distinctive SIC behaviour,[40] the stress softening phenomena of S-DR and S-NR were mainly ascribable to the non-rubber components in their matrices. Interestingly, the stress softening behaviours of S-DR and S-NR were very similar to those observed in rubber vulcanizates filled with high loadings of reinforcing filler, such as carbon black.[58,59] Because of the presence of proteins in dandelion and *Hevea* natural rubbers, the physically aggregated proteins are thought to act as reinforcing fillers in S-DR and S-NR, in agreement with our previous study on *Hevea* natural rubber.[60] Generally, the physical explanations of the Mullins effect in filled rubber vulcanizates include bond rupture, molecular slipping, filler rupture, disentanglement and bond breakage at the filler surface.[57,59] Therefore, the larger degree of stress softening for S-DR and S-NR compared to S-IR and S-GR is probably due to the breakage of the aggregates composed of the higher amount of non-rubber components, particularly the strongly aggregated proteins. Molecular slipping and/or detachment of molecular chains in the physically interactive non-rubber aggregates are also possible.

The effects of physically aggregated non-rubber components were also observed in hysteresis loss and residual strain (Fig. 3). The different area under loading and unloading stress–strain curves in each cycle is an indication of hysteresis loss. The hysteresis loss of S-GR, S-DR, S-NR and S-IR at different cycles and various α_{max} are shown in Fig. 4(a). As expected, the

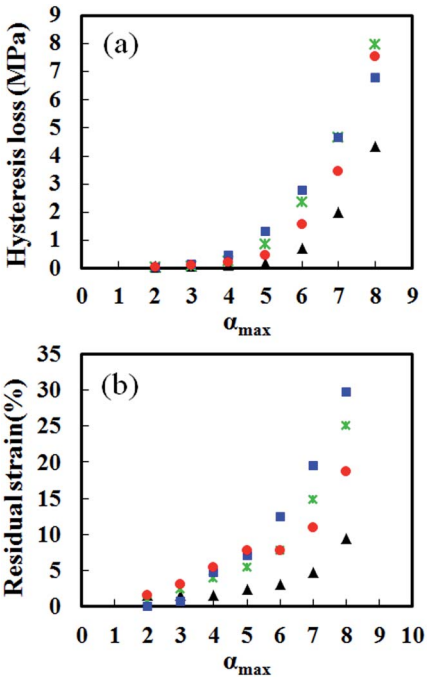

Fig. 4 (a) Hysteresis loss and (b) residual strain of S-GR (●), S-DR (■), S-NR (✖) and S-IR (▲) at different maximum stretching ratios.

hysteresis loss of S-IR was the lowest among the samples, followed by S-GR, S-NR and S-DR, at the same α_{max}, corresponding to the amount of non-rubber components. The residual strains of S-GR, S-DR, S-NR and S-IR at different cycles are shown in Fig. 4(b). Generally, a small but noticeable permanent set was observed at the end of the first unloading curve of the cross-linked rubbers, which reflects the residual strain. The residual strain typically increases upon unloading from an increased α_{max}. S-IR showed a smaller residual strain than the other natural rubber samples, probably because of the absence of non-rubber components. The residual strains of S-GR, S-NR and S-DR, at $\alpha_{max} \leq 5.0$, were similar. Differences became clearer at larger cyclic deformation, with S-DR, which has the highest amount of physically aggregated non-rubber components, showing larger residual strains than S-NR, with S-GR the lowest of the three. This irreversible strain is attributed to the breakage of physically aggregated non-rubber components, which possibly depends on the amount and/or type of non-rubber components inherently presenting in each natural rubber sample.

As discussed above, not only the Mullins effects but also the hysteresis losses and the residual strains of S-GR, S-DR, S-NR and S-IR under cyclic deformation brought us to speculate that the higher-order structure of physically aggregated non-rubber components (*e.g.* morphology of physically aggregated non-rubber components in the rubber matrix) in guayule, dandelion and *Hevea* natural rubbers are probably different depending on the amount and/or kinds of non-rubber constituents. This speculation was supported by the dynamic mechanical analysis shown in the next section.

Dynamic mechanical properties

DMA results, *i.e.*, storage modulus (E') and loss factor (tan δ) over a wide range of temperature from −130 °C to 150 °C for all the samples, are shown in Fig. 5. The dynamic mechanical properties extracted from the plots of S-GR, S-DR, S-NR and S-IR are summarized in Table 1. In the rubbery region, E' of S-DR at 0 °C and 25 °C was slightly higher than those of the other rubbers which decreased in the order of S-NR, S-GR and S-IR. This corresponds to the level of non-rubber components. These results emphasize the reinforcing ability of physically aggregated non-rubber components, particularly proteins, in this temperature range as discussed in the previous section. E' of S-DR became lower when the temperature increased to 125 °C, while that of S-GR slightly increased.

Moreover, E' of S-NR did not change much with increasing temperature. These experimental results clearly show the different temperature dependence behaviours of physically aggregated non-rubber components in each natural rubber sample. The physically aggregated non-rubber components in dandelion natural rubber seem to be diminished under heat compared to the other samples. Moreover, some non-rubber components in dandelion natural rubber may have prevented the sulphur cross-linking reaction. S-DR had the slowest cure progression and lowest maximum torque, which relates to the degree of chemical network chain density among the natural rubber vulcanizates as shown in Fig. 2. This aspect should be further investigated as dandelion natural rubber is applied to the rubber industry, and its analysis will be reported elsewhere in near future.

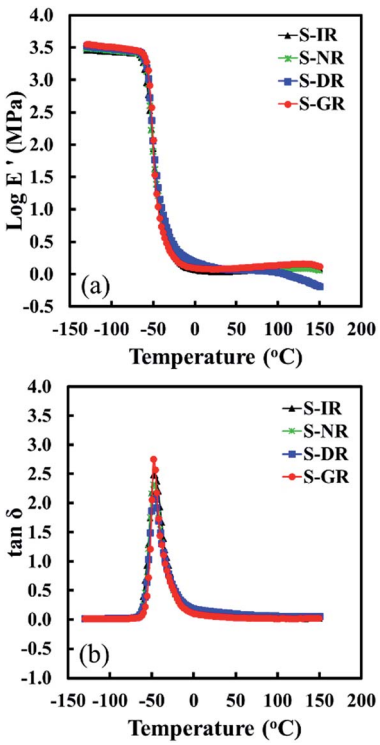

Fig. 5 Temperature dependence of (a) storage modulus (E') and (b) tan δ of S-GR, S-DR, S-NR and S-IR.

Table 1 Dynamic mechanical properties of S-GR, S-DR, S-NR and S-IR

Sample code	E' (MPa)			tan δ peak temperature (°C)	tan δ height	T_g[a] (°C)
	0 °C	25 °C	125 °C			
S-GR	1.26	1.21	1.45	−48	2.8	−59
S-DR	1.55	1.25	0.87	−47	2.1	−58
S-NR	1.35	1.22	1.24	−48	2.3	−58
S-IR	1.17	1.09	1.27	−47	2.5	−59

[a] T_g measured by DSC measurement.

In addition, a reduction of the loss factor (shown as a decrease of height of tan δ peak) was detected in an order of S-GR, S-IR, S-NR and S-DR. The physically aggregated non-rubber components act as reinforcing fillers at temperatures <25 °C restricting the movement of rubber chains, and the degree of rubber chain restriction generally correlated with non-rubber content. However, the higher loss factor of S-GR than S-IR, which is out of order, is possibly due to a plasticization effect of residual long alkyl chain of phospholipids, fatty acids/esters and/or their derivatives in the non-rubber components, promoting the mobility of rubber molecular chains near the glass transition temperature region.

It is also worth noting that the presence of non-rubber components of different types and amounts did not affect the temperature of tan δ peak, which reflects their T_g. All samples had similar T_g of −47 to −48 °C. The four samples also had similar T_g of −58 to −59 °C determined by DSC under static conditions (Table 1). The different T_g values between DMA and DSC were due to the different measurement conditions. As a result, distinct roles of physically aggregated non-rubber components on the mechanical properties become clearer on the basis of their unique higher-order structure as proposed above. What are their higher-order structures in the polyisoprene matrices? The chemical structure of *Hevea* natural rubber[61,62] was shown to comprise of two *trans*-isoprene units connected to long chain *cis*-isoprene units as well as two termini. It was postulated that the α-terminus links with mono- or di-phosphate groups that associate with phospholipids by H-bonding or ionic bonds, whereas the ω-terminus is a dimethylallyl group that links to proteins by H-bonding.[61,62] Ikeda *et al.* supported Tanaka's proposed higher-order structure of *Hevea* natural rubber by means of small-angle neutron scattering (SANS), small-angle X-ray scattering (SAXS) and atomic force microscopy (AFM).[60] In the current study, the Mullins and DMA measurements suggest characteristics of the higher-order structures of guayule and dandelion natural rubbers different to those of *Hevea* natural rubber and of isoprene rubber: the physically aggregated non-rubber components in guayule natural rubber are probably smaller and softer compared to *Hevea* natural rubber due to the absence of proteins, whereas dandelion natural rubber may contain larger aggregated non-rubber components with weaker physical interactions at temperatures above 70 °C than those in *Hevea* natural rubber. In order to confirm this idea, we reconsidered the SIC behaviours

of S-GR, S-DR, S-NR and S-IR under stretching to break[39,40] as explained in the next section.

Tensile properties and SIC behaviours under monotonic uniaxial deformation

Tensile stress–strain curves till the rupture points of S-GR, S-DR, S-NR, and S-IR were obtained during WAXD measurements (Fig. 6). These results are the first direct comparison among stress–strain relationships for sulphur cross-linked *Hevea* natural rubber, guayule natural rubber, dandelion natural rubber and isoprene rubber under identical experimental conditions. Network-chain densities and tensile stresses at $\alpha =$ 5.5 and 7.0, tensile strengths (T_B) and elongation at break (E_B) of S-GR, S-DR, S-NR and S-IR are summarized in Table 2.[39,40] At low stretching ratios, the tensile stresses were comparable among the four samples and corresponded to their network-chain densities. It should be kept in mind that the network-chain densities were measured by swelling in toluene at 25 °C. Thus, the values are supposed to include both the physical and chemical cross-links, because the non-rubber components in natural rubbers are mostly hydrophilic and insoluble in toluene. The differences among tensile stresses were clearly observed with increasing strain. The substantial increases of stress at large deformation were ascribed to their SIC behaviours (Fig. 7), where the oriented index (OI), the oriented amorphous index (OAI) and the crystallinity index (CI) are plotted against stretching ratio for each S-GR, S-DR, S-NR or S-IR, respectively. As shown in the SIC schemata of Fig. S1,† [63–65] orientation of the rubber network-chains starts immediately upon stretching, and it continuously increases with the strain, relating to the increase of OAI values with increasing stretching ratio of all sample as shown in Fig. 7. Then, some relatively short network chains are fully extended upon stretching at a certain strain, and they serve as the starting sites of SIC for the nearest network chains in an amorphous state. The SIC spontaneously increases together with the oriented amorphous segments at larger deformation, corresponding to the progressive increase of both CI and OAI with increasing stretching ratio for all samples (Fig. 7). Also, the total degree of oriented rubber chains, including the oriented crystalline and amorphous segments is explained by increase of OI values with increase of stretching ratio (Fig. 7). These new co-plots between OI, OAI and CI clearly suggest the development of oriented amorphous segments and crystalline phases during stretching in each sample at the same time.

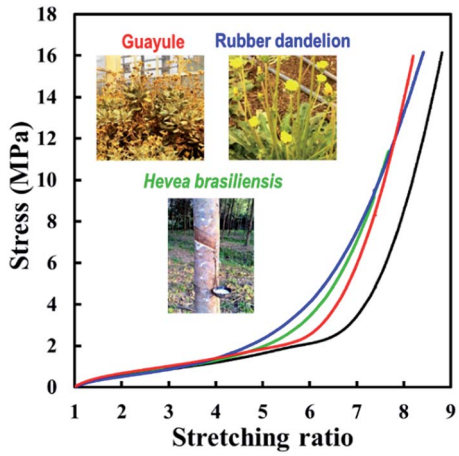

Fig. 6 Stress–strain curves under simple uniaxial deformation of S-GR (—), S-DR (—), S-NR (—) and S-IR (—). Adapted from Fig. 1 and 3 published in ref. 39 and Fig. 1 published in ref. 40.

An orientation rate index and a crystallization rate index were used to compare the four samples. These indexes were obtained from the slope of the increase of OAI and CI from Fig. 7. Note that the orientation rate indexes were only evaluated for the initial stretching regions up to the stretching ratio of $\alpha \leq$ 2.25, due to the complex variations of OAI upon further stretching. It is worth noting that S-GR showed an approximately three times larger orientation rate index than S-IR, S-NR and S-DR at the beginning of stretching, while the others had comparable orientation rate indexes (Table 2). The increase of OAI must have accelerated SIC in S-GR, but the onset of SIC in S-GR was not earlier than those of S-DR and S-NR. Only the initial crystallization rate index of S-GR was larger than those of S-DR and S-NR, and the crystallization rate index of S-GR, in the development of SIC by further stretching, was the fastest among the samples. On the other hand, the onset strain of SIC for S-DR occurred earliest among the samples, and both the initial crystallization rate index and the crystallization rate index in the development of SIC were slowest in S-DR. The characteristics of S-DR may be ascribable to its high amounts of the non-rubber components. The proteins and other non-rubber components such as saccharides in the S-DR rubber matrix may have accelerated the onset of SIC, but they also prevent the development

Table 2 Properties of S-GR, S-DR, S-NR and S-IR

Sample code	Network-chain density $\times 10^5$ (mol cm^{-3})	Stress at $\alpha = 5.5$ (MPa)	Stress at $\alpha = 7.0$ (MPa)	$T_B{}^a$ (MPa)	$E_B{}^b$	Orientation rate index ($\alpha \leq 2.25$) (min^{-1})	Initial crystallization rate index (min^{-1})	Crystallization rate index during developing SIC (min^{-1})
S-GR	9.4	2.1	5.9	16.0	8.3	0.28	0.06	0.33
S-DR	9.7	3.1	7.5	16.2	8.5	0.08	0.01	0.19
S-NR	9.7	2.5	7.0	11.4	7.7	0.07	0.02	0.20
S-IR	8.6	1.9	3.4	16.2	8.8	0.08	0.19	0.27

[a] Tensile strength at break. [b] Elongation at break.

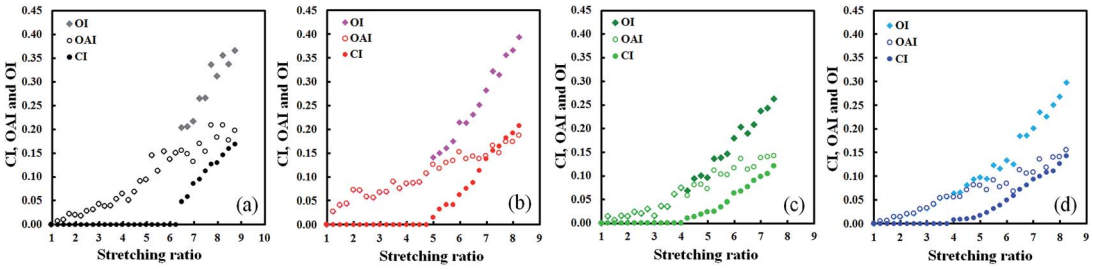

Fig. 7 Plots of OI, OAI and CI of (a) S-IR, (b) S-GR, (c) S-NR and (d) S-DR against stretching ratios. Adapted from Fig. 3 published in ref. 39 and Fig. 2 published in ref. 40.

of SIC. These indexes in S-NR fell between S-GR and S-DR corresponding to the intermediate amount of non-rubber components in *Hevea* natural rubber. The onset strain of S-IR was largest among the samples, and its initial crystallization rate was fastest due to the lack of protein and other non-rubber components. The slightly lower crystallization rate index during developing SIC of S-IR than S-GR was ascribed to the lower stereoregularity of *cis*-1,4-polyisoprene of *ca.* 98% in isoprene rubber than in guayule natural rubber of *ca.* 100%.[16]

The unique SIC behaviour of S-GR may be attributed to the lower amount of non-rubber components, particularly proteins, resulting in the less physical network structure observed. This characteristic feature seems to accelerate the orientation of rubber chains before the onset of SIC much faster than S-NR, S-DR and S-IR. It also seems to develop the SIC more upon further stretching than the others. It is worth noting that only S-GR showed higher CI than OAI when S-GR was stretched over $\alpha = 7.25$ (Fig. 7(b)).

What then causes the increase in the orientation rate index for S-GR? In order to disclose the effects of non-rubber components on the SIC behaviours clearer, the characterization of their SIC behaviours against stress is discussed in the next section.

SIC behaviours characterized by nominal stress

The co-plot of OI, OAI and CI of S-GR, S-DR, S-NR and S-IR against stress, and the magnified section images of each sample in the range of stress ≤6.0 MPa are shown (Fig. 8). The vertical orange dash and double dotted lines indicate a stress at the onset strain of SIC for each sample. Before the onset of SIC, the higher the amount of non-rubber component was, the lower the OAI to load the same stress was detected. This phenomenon clearly suggests the role of non-rubber components as a natural reinforcing filler to load stress. Furthermore, S-IR with no non-rubber components loaded stress of *ca.* 6 MPa through a 27% orientation of both the amorphous segments and the crystalline phase. Interestingly, S-GR also required 28% of total orientation to load the same stress level as S-IR. However, the total amount of orientation to load a stress of *ca.* 6 MPa was *ca.* 21% and 18% for S-NR and S-DR, respectively. Even after the SIC occurred, the role of proteins in non-rubber components as a reinforcing filler was obviously observed. The soft aggregates of the non-rubber

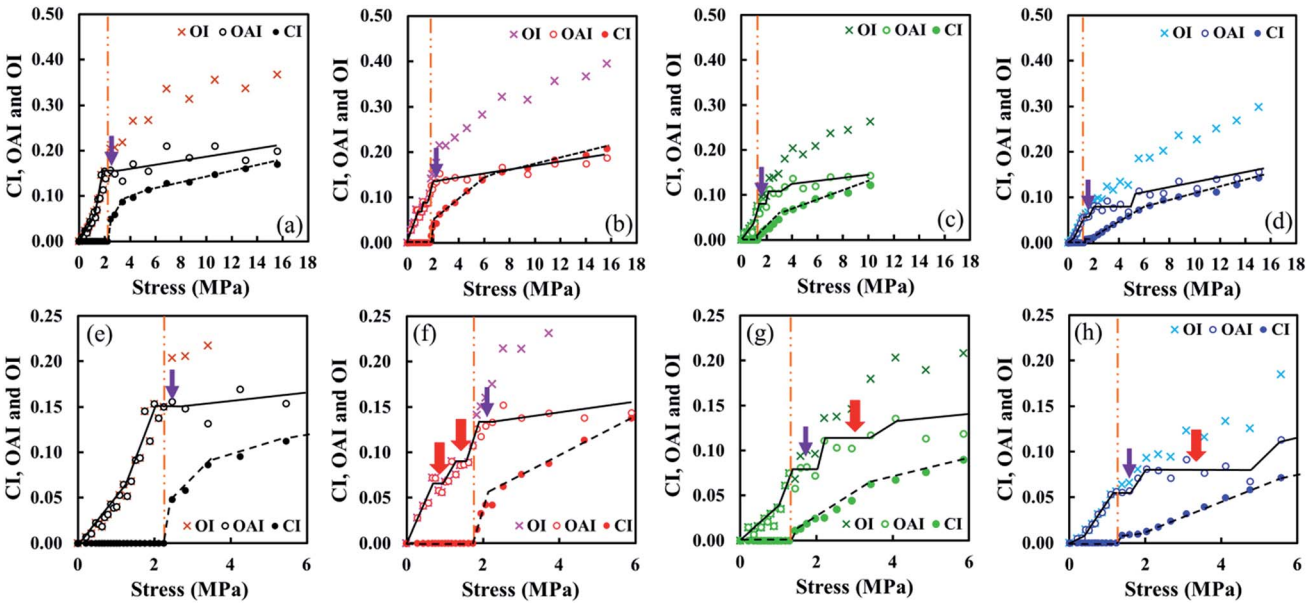

Fig. 8 Co-plot of OI, OAI and CI of (a) S-IR, (b) S-GR, (c) S-NR and (d) S-DR against stress. Magnified images of (a), (b), (c) and (d) are shown in (e), (f), (g) and (h), respectively.

components in guayule natural rubber may have accelerated the rubber chain orientation and further development of SIC in S-GR. In contrast, the physically aggregated non-rubber components in *Hevea* and dandelion natural rubbers accelerated the occurrence of SIC, but also impeded the orientation of rubber chains. Nevertheless, at the same CI, S-DR had the highest stress value and S-IR the lowest among the samples. The stress values of four materials ranged in order as S-DR > S-NR > S-GR > S-IR. The results support the hypothesis that native aggregates such as proteins can act as reinforcing materials in the rubber matrix of S-DR and S-NR at r.t. as previously assumed.[39,60]

It is surprising that a few step-liked regions were seen in the variation of OAI and CI of the four samples (Fig. 8). S-IR had one OAI step near the onset of SIC ($\alpha = ca.$ 2.5 MPa) as indicated by the purple arrow. The CI steeply increased at this region, meaning that some oriented amorphous segments were crystallized. Generally, a slight disorientation of the remained rubber chains occurred by the SIC phenomenon and followed by an increase of entropy for the remained non-crystallized segments from a view point of thermodynamics.[8,66] However, the generated strain-induced crystallites also worked as cross-linking sites both to accelerate and prevent the crystallization. Accordingly, the generation of oriented amorphous segments may have increased and decreased complicatedly. As a result, the step-liked region is supposed to be observed around the onset of SIC in S-IR. This consideration may be acceptable because the step-liked region was observed around their onsets of SIC in all samples, not depending on the amount of non-rubber components. However, it is worth noting that two steps of OAI were detected in S-GR before the onset of SIC as indicated by the red arrows. It may relate to a characteristic of non-rubber components in S-GR to load stresses in this region.

Aggregates of non-rubber components such as the linked fatty acids, their esters or their derivatives in S-GR must have been softer than the aggregates in S-NR and S-DR. Upon stretching, the soft aggregates seemed to play a role to load low stresses before its SIC, but they may have collapsed by further stretching. In fact, the significant increase of OAI was clearly detected before the SIC as shown in Fig. 7(b), 8(b) and (f).

In contrast to S-GR and S-IR, the sulphur cross-linked natural rubbers containing the proteins, *i.e.*, S-NR and S-DR, showed a second step of OAI (red arrows) with increases of CI after their onsets of SIC. The physically aggregated non-rubber components (mainly proteins) in S-NR and S-DR, which are thought to load stresses, impeded the orientation of some rubber chains in S-NR and S-DR. This phenomenon accounts for the decreasing rate of generation of oriented amorphous segments. However, the decrease of CI values in S-NR and S-DR were not seen probably because the crystallites are stable thermodynamically during the propagation of rubber chain arrangement, which is accompanied by minimized free energy as proposed by Flory.[8,67] The length of the second step of OAI for S-NR and S-DR is probably related to their amounts of non-rubber components.

From the considerations mentioned above, speculated structures of physically aggregated non-rubber components in the sulphur cross-linked matrices of purified guayule, dandelion and *Hevea* natural rubbers are proposed, and schematically illustrated in Fig. 9 in comparison to isoprene rubber. Here, the cross-linking networks in each sample were omitted for easier understanding. In isoprene rubber, only polyisoprene chains are presented. The existence of linked fatty acids and their derivatives in the polyisoprene segments of guayule natural rubber is inferred from our data, even after acetone purification. This is proposed to be a mildly restricted physically aggregated

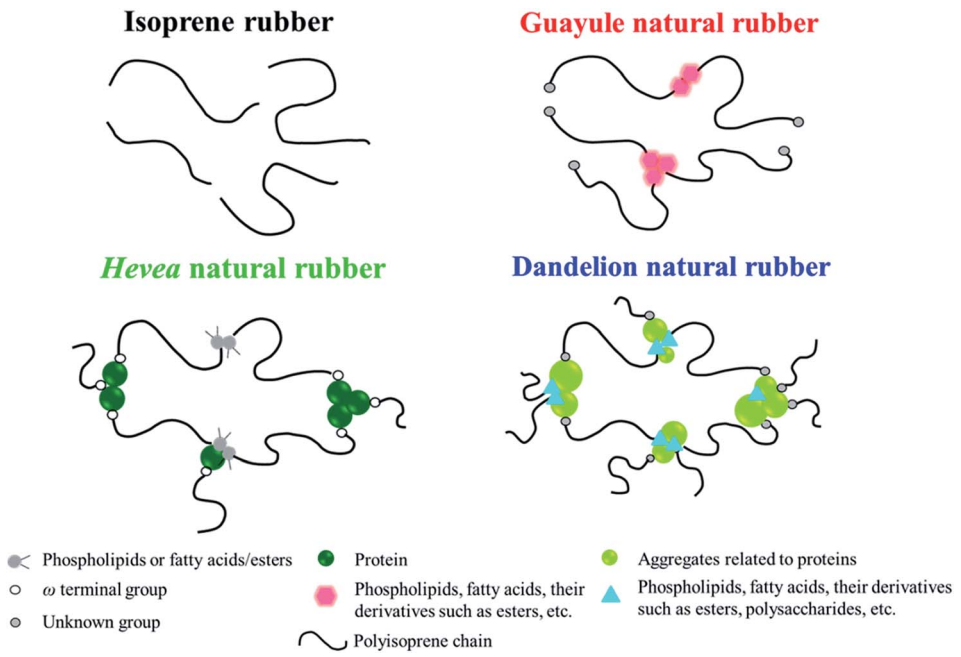

Fig. 9 Speculation of physically aggregates non-rubber components in S-IR, S-GR, S-NR[61] and S-DR.

structure. On the other hand, the presence of proteins, fatty acids/ester, their derivatives, and/or other compounds are predicted to make rigid aggregates, with a high degree of physical interaction, in *Hevea* and dandelion natural rubbers. Note that the aggregated non-rubber components of dandelion natural rubber are judged to act as natural reinforcing filler at r.t., although the thermal stability of the aggregates in S-DR was lower than that of S-NR. This interpretation is supported by two studies reported by Cornish *et al.*[68] and Sakdapipanich *et al.*[69,70] In the former, many proteins with differently higher molecular weights, as well as some similar proteins, were found in dandelion natural rubber latex compared to *Hevea* natural rubber latex. In the latter, an interaction between proteins and non-rubber components with ester groups was predicted to be possible. The polydispersity of molecular weights of proteins in dandelion natural rubber may produce the mixed aggregates of non-rubber components and contribute to the low thermal stability of S-DR (Fig. 5(a)). Alternatively, polysaccharides, such as inulin, in dandelion natural rubber also may be aggregated with the proteins making the aggregates weaker under the heating due to melting of polysaccharides. In fact, inulin was reported to be a main non-rubber component of *ca.* 60 wt% in rubber dandelion roots.[71] Most of the inulin was dissolved in hot water, but some inulin may be retained in the dandelion natural rubber when using the extraction method shown in the Experimental section. The FT-IR spectra of purified dandelion natural rubber after subtraction with isoprene rubber supported this consideration, as seen in Fig. 1(c), where some characteristic peaks of sugars (mono- and/or polysaccharides) were clearly observed. Furthermore, the characteristics of the generated crystallites also may be explained by this hypothesis, as discussed in the next section.

Characteristics of generated crystallites during deformation

(i) Variation of SIC parameters of generated crystallites upon stretching. Fig. 10(a) and (b) present the crystallite size of S-GR, S-DR, S-NR and S-IR estimated from the 200 (L_{200}), 120 (L_{120}) and 002 (L_{002}) reflections against stretching ratio, respectively. The contents of non-rubber components and the physical interactions between the aggregates of non-rubber components in each rubber slightly affected the L_{200} and L_{120}. In contrast, they significantly influenced the L_{002} values, which must relate to the length of starting sites of SIC, orientation of rubber chains and development of crystallites in the stretching direction. The rubbers were clearly separated into two groups (Fig. 10(b)), one group containing S-IR and S-GR, and the other, S-NR and S-DR. S-IR and S-GR had larger L_{002} values than S-NR and S-DR. This indicates that the starting sites of SIC in S-IR and S-GR seem to have a role as a template of crystallization for neighbouring long amorphous network chains.[63–65] The template crystallization must be much more developed in S-IR and S-GR due to none or less hard non-rubber components, respectively, than in S-NR and S-DR. An example of the template crystallization of cross-linked natural rubber is illustrated in Fig. S1.†[63–65] *In situ* epitaxial crystallization onto the template crystallization of S-IR and S-GR seems to develop more

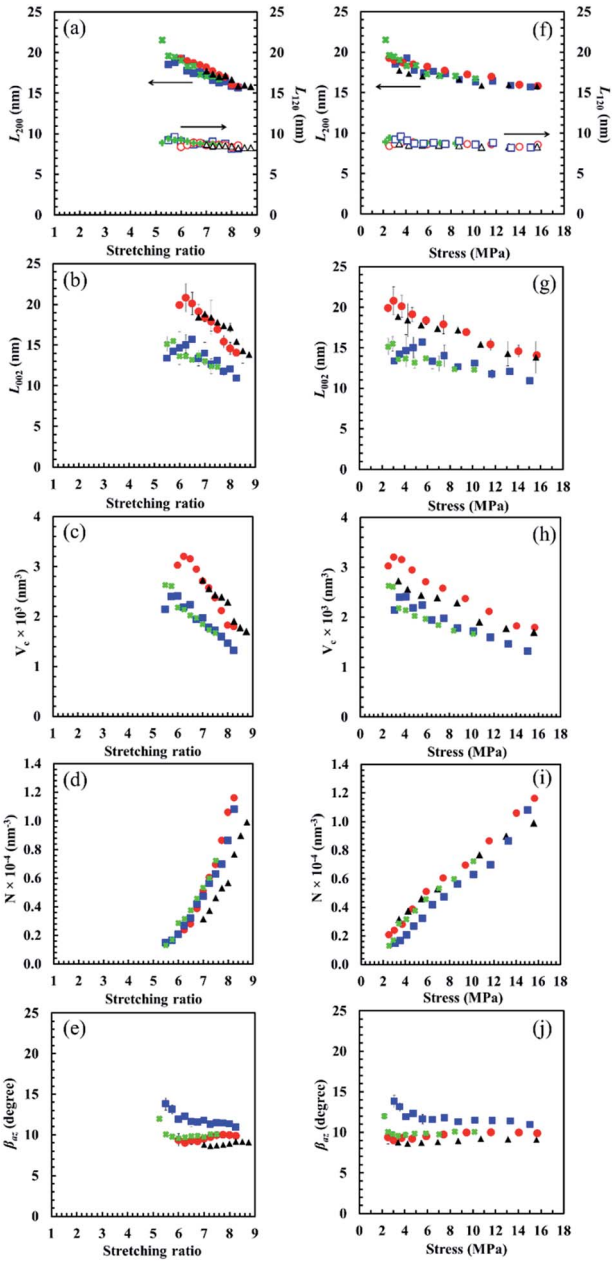

Fig. 10 Variation of apparent crystallite size (a) L_{200}, L_{120}, (b) L_{002}, (c) average volume of crystallites, (d) index of average number of crystallites and (e) orientation fluctuation of crystallites of S-GR (●, ○), S-DR (■, □), S-NR (×, +) and S-IR (▲, Δ) against stretching ratio (adapted from Fig. 4 published in ref. 39 and Fig. 3 published in ref. 40). The parameters in (a)–(e) plotted against stress for all samples are shown in (f)–(j), respectively.

spontaneously than in S-NR and S-DR, leading to the bigger crystallites which are more highly oriented to the stretching direction in the former group than in the latter group. Especially, the low physical branching molecular structure composed of *cis*-1,4-polyisoprene segments in guayule natural rubber accelerates the template crystallization upon stretching. The second group, of S-DR and S-NR, also shows a few differences between the two rubbers. For example, the weaker physically aggregated non-rubber components in S-DR than in S-NR

cause a slightly larger L_{002} near the onset of SIC than in S-NR, even though the non-rubber components of the former were greater than in the latter. Probably, the weaker physical interaction of non-rubber aggregates in S-DR accelerates the orientation of rubber chains and allows the epitaxial crystallization onto the template prior to the breaking of non-rubber aggregates at large deformation.

As a result, the average crystallite volume (V_c calculated from apparent crystallite sizes in three reflections) decreased in the order of S-GR > S-IR > S-DR > S-NR, respectively, corresponding to their values of L_{002}. The orientation fluctuation of crystallites (β_{az}) decreased in the order of S-DR > S-NR > S-GR > S-IR with increasing the stretching ratio, and the smaller the β_{az} the better the orientation in the stretching direction. The high amounts of non-rubber components in natural rubbers significantly affected the β_{az}.

It is also worth noting that the average numbers of crystallites (N) were similar among S-GR, S-DR and S-NR, but was significantly lower in S-IR. Under large deformation, the number of starting sites for generating SIC, *i.e.* the number of templates for SIC, has been presumed to be governed by various factors such as the chemical and physical cross-linking of the non-rubber components, trapped entanglements, a degree of stereoregularity, and so on. However, from the viewpoint of template crystallization, the low proportion of *cis*-configurations in isoprene rubber chains may be the main factor causing the smaller N in S-IR compared to the three natural rubbers. The comparison of these four cross-linked samples explains the mechanism of template crystallization clearly. This concept of SIC for natural rubber gives rise to a unique new arena of polymer crystallization distinct from crystallization due to nucleation. SIC is necessarily caused by externally applied deformation, absolutely not by chance, while nucleation is a stochastic process.

(ii) Variation of SIC parameters of generated crystallites against stress. The effects of non-rubber components on the generated strain-induced crystallite behaviours becomes clearer when even the SIC parameters were considered at the same stress (Fig. 10(f)–(j)). The characteristics of the physically aggregated components in each natural rubber sample were found to mainly affect their apparent crystallite size parallel to the stretching direction, L_{002}. As explained above, the L_{002} of S-GR and S-IR were larger than those of S-DR and S-NR due to the acceleration of rubber chain orientation by softer non-rubber aggregates. However, the slightly larger L_{002} of S-GR than S-IR is ascribable to the higher stereoregularity of *cis*-configuration of guayule natural rubber than isoprene rubber. These similar tendencies were also detected in the plot of V_c against stress (Fig. 10(h)), in which the difference between S-GR and S-IR became clear. In addition, the lowest average number of crystallites in S-DR among the four at the same stress (Fig. 10(i)) indicates that the highest amount of non-rubber components, especially proteins, in dandelion natural rubber caused the greatest impendence of rubber chain orientation in the stretching direction. This explanation is strongly supported by the highest β_{az} of S-DR among the four rubbers (Fig. 10(j)).

The proposed behaviours of the generated crystallites in S-GR, S-DR, S-NR and S-IR at the same stress of approximately 6 MPa are illustrated in Fig. 11. The distinct effects of non-rubber components on the different behaviours of generated crystallites among the samples are clearly observed from the plots of their SIC behaviours against nominal stress (Fig. 10). These data strongly support our idea that non-rubber components play a role as reinforcing fillers in the rubber matrices. The tendency of SIC behaviours to be affected by non-rubber components is similar to the effect of conventional fillers on S-GR, S-DR, S-NR and S-IR, which can also lead to earlier SIC onset.[11,12] Additionally, the smaller crystallite sizes and volume

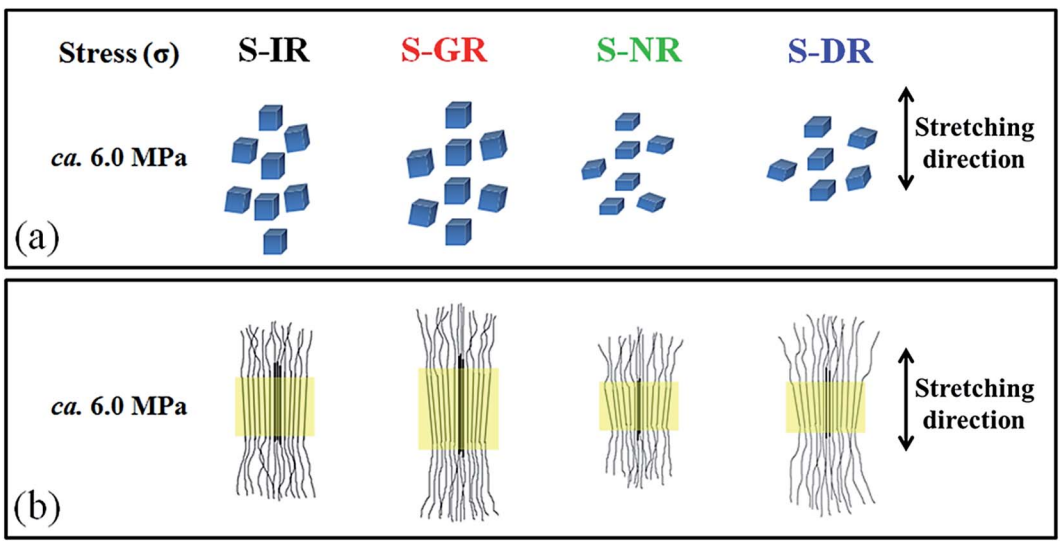

Fig. 11 (a) Schematic drawings of the morphologies at the same stress for the generated crystallites in S-IR, S-GR, S-NR and S-DR, respectively. (b) Two-dimensional images for each generated crystallite at the same stress in S-IR, S-GR, S-NR and S-DR. The yellow parts show the crystallites. Thick lines in the centers of each crystallites represent starting sites for SIC.

but higher orientation fluctuation of crystallites of the samples with increasing the amounts of non-rubber are clear (Fig. 11). The unique point of rubber reinforcement by non-rubber components is that the number of crystallites decreased as the amount of physically aggregated non-rubber components (especially the proteins) increased. This is may be due to stronger interactions by H-bonding and/or ionic interactions between physically aggregated non-rubber components, leading to a significant impedance of rubber chains orientation compared to the conventional filler system. Nevertheless, both the non-rubber components and the generated crystallites are responsible for loading stress, which is confirmed by the stress dependence of lattice constants (Fig. 12) as described in the next section.

(iii) Deformation of crystal lattice with the nominal stress. Lattice constants were estimated from each WAXD pattern during the deformation process by using the least-squares regression method.[8,54] This is the first report showing comparative lattice constants among S-GR, S-DR, S-NR and S-IR. The rectangular unit cell proposed by Nyburg[72] was assumed at first, and estimated values of the lattice constants and the volume of the unit cell for all the samples were plotted against stress (Fig. 12). The unit cell contracts along *a* and *b* directions (perpendicular to the applied stress direction) and elongates in the *c* direction (parallel to the applied stress direction). The deformation of the unit cell exhibited a near linear relationship with nominal stress for all four samples. Again, these results indicate that the strain-induced crystallites are responsible for the load in all samples. However, the decreasing lattice constants in the *a*- and *b*-axes, as well as increasing lattice constants in the *c*-axis for S-DR and S-NR, indicated that the lattice deformation rate tended to be slower than those in S-GR and S-IR. The smaller stress dependence of lattice constants for the S-DR and S-NR indicates that the stress to the crystallites was decreased by the presence of the higher amount of physically aggregated non-rubber components, especially proteins. The volume of the unit cell calculated from the lattice constants slightly decreased with the increase of tensile stress. At a given stress, all rubber samples had comparable lattice constants, *i.e.*, *a*, *b* and *c*-axes. Nevertheless, slight differences of each parameter among the samples were observed at low deformation. The effect of physically aggregated non-rubber components on lattice constants of sulphur cross-linked rubbers predominates in this range. However, these differences disappear under larger deformation, and all lattice constants become very similar, due to the rupture of aggregated non-rubber components.

The effect of non-rubber components on the unit cell size in S-GR, S-DR, S-NR and S-IR was clear, and was impacted by the polymer *cis* content. Thus, S-GR may have a perfect closely packed unit cell, resulting in the overall smaller unit cell volume. The unit cells in S-DR and S-NR may be less closely packed because of the impedance by higher non-rubber contents, leading to the larger overall unit cell volumes observed in S-DR and S-NR than in S-GR. Ultimately, the largest unit cell volume of S-IR among the samples is ascribable to the lower regularity of *cis* configuration of isoprene rubber than in

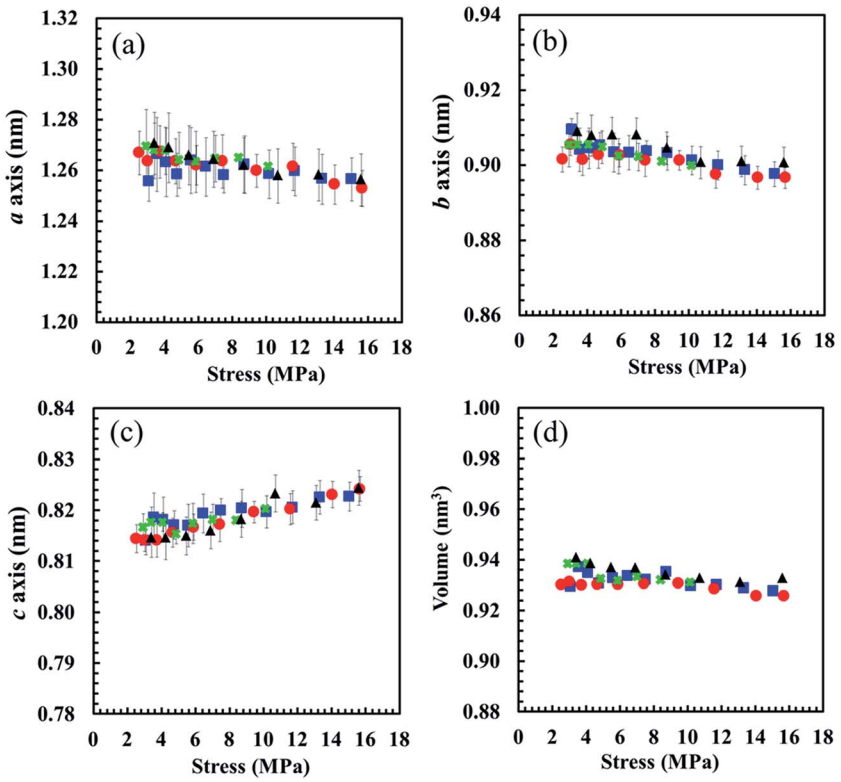

Fig. 12 Deformation of crystal lattice in (a) *a* axis, (b) *b* axis, (c) *c* axis and (d) volume of unit cell with nominal stress of S-GR (●), S-DR (■), S-NR (×) and S-IR (▲).

the other natural rubbers samples. Thus, crystal unit cell of the sulphur cross-linked rubbers seemed to be most affected by the stereoregularity of *cis*-1,4-polyisoprene and impurities differences.

Conclusion

The roles of non-rubber components in S-GR and S-DR were revealed by the first direct comparison of Mullins effect and dynamic mechanical analysis. By comparing the S-NR and S-IR results, the non-rubber components were found to aggregate and work as reinforcing fillers in the rubber matrices in the low temperature region below *ca.* 25 °C. The physically aggregated non-rubber components reinforcing S-GR showed very low stress softening, hysteresis loss and residual strain. Such properties were considerably higher in S-DR which was reinforced with the high protein aggregates. In addition, S-DR showed stronger temperature dependence of storage modulus than the other samples. Some of non-rubber components in dandelion natural rubber may have melted and/or softened at high temperature, or prevented the sulphur cross-linking reaction. This aspect should be better understood for applications of dandelion natural rubber to the rubber industry.

The strain-induced crystallization (SIC) behaviours related to the nominal stresses clearly supported the distinct role of physically aggregated non-rubber components in each sample. The relationship of oriented amorphous index to stress before and after the onsets of SIC, led to our proposed higher-order structures of physically aggregated non-rubber components in guayule and dandelion natural rubber matrices (Fig. 9). The proposed structures consistently explain the characteristics of crystallites generated upon stretching in all samples.

Not only the amount of non-rubber components in natural rubbers but also the characteristics of aggregates of non-rubber components should be taken into account when using guayule and dandelion natural rubbers as alternatives to *Hevea* natural rubber. The purity of the alternative natural rubbers may be one of the important keys for controlling mechanical properties of their vulcanizates in order to produce consistently high performance natural rubber materials for the rubber industry.

Conflicts of interest

There are no conflicts to declare.

Acknowledgements

This work was supported by JST ALCA program (2015 -) and the 48th Kurata Grants to Y. I. The WAXD experiment was performed at the BL-40XU in the SPring-8 with the approval of the Japan Synchrotron Radiation Research Institute (JASRI) (Proposal No. 2015A1872, 2015B1814). The authors thanks Prof. Dr S. Kohjiya, Dr A. Tohsan, Dr T. Phakeeree and Mr Y. Sakaki for their useful comments.

References

1 L. Bateman, *The Chemistry and Physics of Rubber-like Substances*, Maclaren & Sons, London, 1963.
2 A. D. Robert, *Natural Rubber Science and Technology*, Oxford University Press, Oxford, 1988.
3 J. E. Mark and B. Erman, *The Science and Technology of Rubber*, Elsevier Academic Press, Oxford, 3rd edn, 2005.
4 S. Kohjiya, *Natural Rubber: From the Odyssey of Hevea Tree to the Age of Transportation*, Smithers Rapra Publications, Shrewsbury, 2015.
5 Y. Ikeda, A. Tohsan and S. Kohjiya, in *Sustainable Development Processes, Challenges and Prospects*, ed. D. Reyes, Nova Science Publishers, Inc, New York, 2015, ch. 3, pp. 65–85.
6 S. Murakami, K. Senoo, S. Toki and S. Kohjiya, *Polymer*, 2002, **43**, 2117–2120.
7 S. Toki, I. Sics, S. Ran, L. Liu, B. S. Hsiao, S. Murakami, K. Senoo and S. Kohjiya, *Macromolecules*, 2002, **35**, 6578–6584.
8 M. Tosaka, S. Murakami, S. Poompradub, Y. Ikeda, S. Kohjiya, S. Toki, I. Sics and B. S. Hsiao, *Macromolecules*, 2004, **37**, 3299–3309.
9 Y. Ikeda, Y. Yasuda, S. Makino, S. Yamamoto, M. Tosaka, K. Senoo and S. Kohjiya, *Polymer*, 2007, **48**, 1171–1175.
10 Y. Ikeda, Y. Yasuda, K. Hijikata, M. Tosaka and S. Kohjiya, *Macromolecules*, 2008, **41**, 5876–5884.
11 S. Poompradub, M. Tosaka, S. Kohjiya, Y. Ikeda, S. Toki, I. Sics and B. S. Hsiao, *Chem. Lett.*, 2004, **33**, 220–221.
12 S. Poompradub, M. Tosaka, S. Kohjiya, Y. Ikeda, S. Toki, I. Sics and B. S. Hsiao, *J. Appl. Phys.*, 2005, **97**, 103529.
13 Y. Ikeda and A. Tohsan, *Colloid Polym. Sci.*, 2014, **292**, 567–577.
14 S. Kohjiya and Y. Ikeda, *Chemistry, Manufacturing and Applications of Natural Rubber*, Woodhead Publishing, Cambridge, 2014.
15 D. C. Blackley, *Polymer Latices: Science and Technology Volume 1: Fundamental Principal*, Springer, Netherland, 1997.
16 Engineering Department of Japan Synthetic Rubber (JSR) Corporation, *JSR Handbook*, JSR Corporation, Tokyo, 3rd edn, 1988.
17 R. Clamroth and T. Kempermann, *Polym. Test.*, 1986, **6**, 3–35.
18 M. J. W. Cock, M. Kenis and R. Wittenberg, *Natural Rubber: Biosecurity and Forests: An Introduction: with Particular Emphasis on Forest Pests*, Rubber Forestry Department, Food and Agricultural Organization (FAO) of the United Nations, Rome, 2003.
19 R. E. Schultes, *Bot. Rev.*, 1970, **36**, 197–276.
20 P. J. George and J. C. Kuruvilla, *Natural Rubber: Agromanagement and Crop Processing*, Rubber Research Institute of India, Kottayam, 2000.
21 F. E. Lloyd, *Guayule (Parthenium argentatum Gray): A Rubber-Plant of the Chihuahuan Desert*, Carnegie Institution of Washington, Washington D. C., 1911.
22 W. W. Gordon and B. J. Stevenson, *Russian Dandelion (KOK-SAGHYZ): An Emergency Source of Natural Rubber*, U.S. Department of Agriculture, Washington D. C., 1947.

23 National Academy of Sciences, *Guayule: An Alternative Source of Natural Rubber*, Books for Business, New York, 2002, Originally published in 1977.
24 J. B. van Beilen and Y. Poirier, *Crit. Rev. Biotechnol.*, 2007, **27**, 217–231.
25 P. Venkatachalam, N. Geetha, P. Sangeetha and A. Thulaseedharan, *Afr. J. Biotechnol.*, 2013, **12**, 1297–1310.
26 M. Bomgardner, *Chem. Eng. News*, 2016, **94**, 28–29.
27 H. Mooibroek and K. Cornish, *Appl. Microbiol. Biotechnol.*, 2000, **53**, 355–365.
28 L. F. Ramos-De Valle, *Rubber Chem. Technol.*, 1981, **54**, 24–33.
29 L. F. Ramos-De Valle and M. Montelongo, *Rubber Chem. Technol.*, 1978, **51**, 863–871.
30 D. S. Winkler, H. J. Schostarez and H. L. Stephens, *Rubber Chem. Technol.*, 1977, **50**, 981–987.
31 C. S. Barrera and K. Cornish, *Ind. Crops Prod.*, 2016, **86**, 132–142.
32 I. S. Choi and C. M. Roland, *Rubber Chem. Technol.*, 1996, **69**, 591–599.
33 P. G. Santangelo and C. M. Roland, *Rubber Chem. Technol.*, 2003, **76**, 892–898.
34 S. M. A. Monadjemi, C. M. McMahan and K. Cornish, *J. Res. Updates Polym. Sci.*, 2016, **5**, 87–96.
35 L. S. Porter and H. L. Stephens, *Rubber Chem. Technol.*, 1979, **52**, 361–376.
36 Y. Shimimura, J. L. White and J. E. Spruiell, *J. Appl. Polym. Sci.*, 1982, **27**, 3553–3567.
37 I. Choi and C. Roland, *Rubber Chem. Technol.*, 1997, **70**, 202–210.
38 S. Musto, V. Barbera, M. Maggio, M. Mauro, G. Guerra and M. Galimberti, *Polym. Adv. Technol.*, 2016, **27**, 1082–1090.
39 Y. Ikeda, P. Junkong, T. Ohashi, T. Phakkeeree, Y. Sakaki, A. Tohsan, S. Kohjiya and K. Cornish, *RSC Adv.*, 2016, **6**, 95601–95610.
40 P. Junkong, T. Ohashi, T. Phakkeeree, Y. Sakaki, A. Tohsan, K. Cornish and Y. Ikeda, *Kautsch. Gummi Kunstst.*, 2017, **7–8**, 38–43.
41 S. Kohjiya, M. Tosaka, M. Furutani, Y. Ikeda, S. Toki and B. S. Hsiao, *Polymer*, 2007, **48**, 3801–3808.
42 S. Amnuaypornsri, J. Sakdapipanich, S. Toki, B. S. Hsiao, N. Ichikawa and Y. Tanaka, *Rubber Chem. Technol.*, 2008, **81**, 753–766.
43 S. Amnuaypornsri, S. Kawahara, S. Toki, B. S Hsiao, M. Hikosaka, J. Sakdapipanich and Y. Tanaka, *Kautsch. Gummi Kunstst.*, 2012, **65**, 46–50.
44 S. Amnuaypornsri, S. Toki, B. S. Hsiao and J. Sakdapipanich, *Polymer*, 2012, **53**, 3325–3330.
45 T. F. Banigan, A. J. Verbiscar and C. W. Weber, *J. Agric. Food Chem.*, 1982, **30**, 427–431.
46 T. F. Banigan, A. J. Verbiscar and T. A. Oda, *Rubber Chem. Technol.*, 1982, **55**, 407–415.
47 W. W. Schloman Jr, R. A. Hively, A. Krishen and A. M. Andrews, *J. Agric. Food Chem.*, 1983, **31**, 873–876.
48 L. T. Black, G. E. Hamerstrand, F. S. Nakayama and B. A. Rasnik, *Rubber Chem. Technol.*, 1983, **56**, 367–371.
49 O. P. Sidhu, N. Ratti and H. M. Behl, *J. Agric. Food Chem.*, 1995, **43**, 2012–2015.
50 C. McMahan, D. Kostyal, D. Lhamo and K. Cornish, *J. Appl. Polym. Sci.*, 2015, **132**, 42051.
51 N. T. Thuong, O. Yamamoto, P. T. Nghia, K. Cornish and S. Kawahara, *Polym. Adv. Technol.*, 2017, **28**, 303–311.
52 M. Morton, *Rubber Technology*, USA, Ohio, 3rd edn, 1999.
53 P. J. Flory, *J. Chem. Phys.*, 1950, **18**, 108–111.
54 M. Tosaka, S. Kohjiya, S. Murakami, S. Poompradub, Y. Ikeda, S. Toki, I. Sics and B. S. Hsiao, *Rubber Chem. Technol.*, 2004, **77**, 711–723.
55 L. Mullins, *Rubber Chem. Technol.*, 1948, **21**, 281–300.
56 J. A. C. Harwood and A. R. Payne, *J. Appl. Polym. Sci.*, 1966, **10**, 1203–1211.
57 J. Diani, B. Fayolle and P. Gilormini, *Eur. Polym. J.*, 2009, **45**, 601–612.
58 J. A. C. Harwood, L. Mullins and A. R. Payne, *J. Appl. Polym. Sci.*, 1965, **9**, 3011–3021.
59 R. Diaz, J. Diani and P. Gilormini, *Polymer*, 2014, **55**, 4942–4947.
60 T. Karino, Y. Ikeda, Y. Yasuda, S. Kohjiya and M. Shibayama, *Biomacromolecules*, 2007, **8**, 693–699.
61 Y. Tanaka, H. Sato and A. Kageyu, *Rubber Chem. Technol.*, 1983, **56**, 299–303.
62 J. Tangpakdee and Y. Tanaka, *J. Nat. Rubber Res.*, 1977, **12**, 112–119.
63 S. Kohjiya and Y. Ikeda, *Crystallization of natural rubber, Paper presented at the 191st Technical Meeting*, Rubber Division, American Chemical Society, Beachwood, OH, Akron, 25 April 2017.
64 Y. Ikeda, A. Kato, S. Kohjiya and Y. Nakajima, *Rubber Science: A Modern Approach*, Springer, Singapore, 2017.
65 S. Kohjiya, P. Junkong and Y. Ikeda, *Kautsch. Gummi Kunstst.*, 2017, **10**, 38–48.
66 B. Amram, L. Bokobza, L. P. Queslel and L. Monnerie, *Polymer*, 1986, **27**, 877–882.
67 P. J. Flory, *J. Chem. Phys.*, 1947, **15**, 397–408.
68 K. Cornish, W. Xie, D. Kostyal, D. Shintani and R. G. Hamilton, *J. Biotechnol. Biomater.*, 2015, **5**, 1000207.
69 K. Nawamawat, J. Sakdapipanich, C. C. Ho, Y. Ma, J. Song and J. G. Vancso, *Colloids Surf., A*, 2011, **390**, 157–166.
70 J. Sakdapipanich, R. Kalah, A. Nimpaiboon and C. C. Ho, *Colloids Surf., A*, 2015, **466**, 100–106.
71 D. A. Ramirez-Cadavid, K. Cornish and F. C. Michel Jr, *Ind. Crops Prod.*, 2017, **107**, 624–640.
72 S. C. Nyburg, *Acta Crystallogr.*, 1954, **7**, 385–392.

